GT2008-51411

ESTABLISHING A METHODOLOGY FOR RESOLVING CONVECTIVE HEAT TRANSFER FROM COMPLEX GEOMETRIES

J. Ostanek and K. Thole
Mechanical and Nuclear Engineering Department
The Pennsylvania State University
University Park, PA

J. Prausa and A. Van Suetendael
United Technologies-Pratt & Whitney
Military Engines
W. Palm Beach, FL

ABSTRACT

Current turbine airfoils must operate at extreme temperatures, which are continuously driven higher by the demand for high output engines. Internal cooling plays a key role in the longevity of gas turbine airfoils. Ribbed channels are commonly used to increase heat transfer by generating turbulence and to provide a greater convective surface area. Because of the increasing complexity in airfoil design and manufacturing, a methodology is needed to accurately measure the convection coefficient of a rib with a complex shape. Previous studies that have measured the contribution to convective heat transfer from the rib itself have used simple rib geometries. This paper presents a new methodology to measure convective heat transfer coefficients on complex ribbed surfaces. The new method was applied to a relatively simple shape so that comparisons could be made with a commonly accepted method for heat transfer measurements.

A numerical analysis was performed to reduce experimental uncertainty and to verify the lumped model approximation used in the new methodology. Experimental measurements were taken in a closed-loop channel using fully rounded, discontinuous, skewed ribs oriented 45° to the flow. The channel aspect ratio was 1.7:1 and the ratio of rib height to hydraulic diameter was 0.075. Heat transfer augmentation levels relative to a smooth channel were measured to be between 4.7 and 3 for Reynolds numbers ranging from 10,000 to 100,000.

NOMENCLATURE

AR   channel aspect ratio H/W
Bi   Biot number
e   rib height
D_h hydraulic diameter
H   channel height (ribbed walls)
h   heat transfer coefficient based on bulk temperature
k   thermal conductivity
ℓ contact length between rib and endwall
L   length of rib less rounded ends
P   rib pitch
Q   heat transfer
Nu   Nusselt number based on D_h
Nu_o baseline Nusselt number, $Nu = 0.023 \cdot Re^{0.8} Pr^{0.4}$
Pr   Prandtl number
Re   Reynolds number based on U, D_h and ν
s   spanwise distance
s′   spanwise distance aligned with rib
T   temperature
U   average velocity in unobstructed channel
w   rib width
W   channel width (non-ribbed walls)
x   streamwise distance
x′   streamwise distance, orthogonal to s′
y   direction vector mutually orthogonal to x and s

Greek

α   rib angle of attack
ν   dynamic viscosity
ρ   density
θ   circumferential location or dimensionless temperature

Subscripts

0   unobstructed duct baseline condition
∞   freestream value
bc   boundary condition applied to computational model
rib   measured coefficients using internal rib temperatures

INTRODUCTION

Gas turbine engines are used in many applications ranging from aircraft and marine propulsion to power generation. To meet demands for increased efficiency, gas turbines are designed to operate with higher combustion temperatures. Increased combustion temperatures are beneficial for efficiency and power production. Increased temperatures, however, are problematic for components downstream of the combustion chamber. First stage turbine vanes and subsequent turbine blades are frequently exposed to temperatures in excess of the components' melting temperature. Therefore, turbine components rely on various thermal management techniques.

Turbine airfoils are commonly cast with internal passageways that provide an avenue for a cooling medium, such as compressor bypass air, to flow through. To enhance heat transfer to the bypass air, extended surfaces such as ribs and pin-fins are placed along the walls of the internal passageways. These enhancement features increase convective surface area, interrupt thermal boundary layers, and increase turbulent transport in the flow. Obstructing the flow using these features, however, also causes additional pressure loss through the channels. A considerable amount of research has been performed to design internal cooling passages that provide sufficient heat transfer while minimizing pressure loss through the channels.

There are numerous methodologies to quantify the convective heat transfer from the endwalls of a ribbed channel. Alternatively, there are few studies that directly address the convective heat transfer contribution from a specific rib turbulator. Furthermore, previous methods quantify the convection coefficient from simple rib geometries while manufacturing advancements have led to increasingly complex rib shapes. This paper presents a methodology to determine the contribution of rib surfaces to the convective heat transfer for a ribbed channel. Although the aim was to develop a method for complex rib shapes, the new method was applied to a simple rib geometry so the method could be validated with a commonly accepted method for measuring heat transfer coefficients.

PREVIOUS STUDIES

Many previous studies have addressed the challenges of internal cooling with ribbed channels. Because this paper presents a methodology to quantify rib heat transfer, the scope of literature includes any method of measuring internal heat transfer coefficients.

Since the 1980's, researchers have constructed test models from thermally conductive materials, such as copper. The model is typically uniformly heated and insulated from ambient conditions. After reaching steady-state, a single thermocouple measurement is collected representing the average temperature of the convective surface [1-6]. The Biot number can be used as a first order approximation of the uniformity of the temperature field within the model. The high thermal conductivity of copper drives the Biot number well below unity for convection coefficients common to internal cooling applications. The

average surface temperature translates to a region-averaged convection coefficient. Generally, this method will not allow for the discretization of the endwall contribution from the rib contribution. However, Metzger et al. [7, 8] used this approach to collect row-resolved heat transfer coefficients within a pin-fin array. By replacing copper pin-fins with adiabatic pins, Metzger et al. [7, 8] were able to discretize the endwall contribution from the pin contribution. For the scope of this paper, this methodology is difficult to implement when the turbulators take a complex shape. Machining a unique copper model for specific test geometries is neither time nor cost effective.

Similar to this approach, Chyu et al. [9, 10] used the lumped model approach by placing heated aluminum pin-fins within adiabatic walls. Taslim et al. [11-13] and Korotky et al. [14] placed a heated copper rib on top an insulated endwall and collected the area-averaged rib temperature with three thermocouples. References [9-14] show the lumped model approach for individual turbulators as an alternative to the discretization of turbulator contribution used by Metzger et al. [7, 8]. This lumped model approach will deliver a slightly more resolved data set. Area-averaged heat transfer coefficients on pin-fin and rib surfaces were presented. As with previous copper channels or channel sections, machining individual complex shaped turbulators is time and cost consuming.

A reliable alternative to the lumped approximation involves applying a uniform heat flux to the convective surfaces within the cooling channel. Probing the surface of the heater for local temperature measurements will yield local heat transfer coefficients. Chang et al. [15, 16] have used this method to collect a slightly more resolved data set than the previous methodologies. Chang et al. [15, 16] covered the endwall of a ribbed channel with a piece of forged stainless steel, which included the shapes of the rib turbulators. A low thermal conductivity material was placed behind the stainless steel heater to prevent losses through the backside of the heater. Similarly, the same apparatus and measurement methodology has been used to obtain the convection coefficient from pin-fin surfaces by Ames et al. [17]. The same experimental apparatus can be used in conjunction with other measurement methodologies such as infrared (IR) imaging [18, 19] or with steady-state thermochromatic liquid crystals (TLC) [20, 21]. Both of these imaging methodologies have the potential to deliver the spatially resolved heat transfer coefficients on both the endwall and turbulator surfaces. Regardless of the measurement method, it is difficult to implement a surface heater on complex geometries.

Using TLC in a transient manner is another methodology of obtaining spatially resolved convection coefficients [22-25]. In this application, the thermal boundary condition on the endwalls is approximated as point-wise, one-dimensional, transient conduction normal to the exposed surface condition. Therefore, the time response of the TLC paint can be measured and translated into a convection coefficient. The one-dimensional conduction boundary condition, however, is limited based on the fact that the rib surface has multi-dimensional thermal

Copyright © 2008 by ASME

loading through the rib. Unless the conduction through the turbulator can be accounted for, using liquid crystals in a transient test yields questionable coefficients on complex surfaces. Han et al. [20] showed that collecting heat transfer data on the rib-tops alone will under predict the overall area-averaged heat transfer coefficient. The authors go on to say that the rib sides, when considering a square rib cross section, contribute significantly to the overall area-averaged heat transfer. Similar to transient TLC, Naphthalene sublimation is a methodology that can spatially resolve the convection coefficient from a flat endwall [26-29]. Coating the convective surfaces with Naphthalene is analogous to a constant temperature boundary condition. And, any surface uncoated is analogous to an adiabatic surface. Using the mass transfer analogy, the Sherwood ratio can be calculated by measuring the amount of Naphthalene that has left the surface. Using Naphthalene sublimation on complex geometries introduces complexities in applying a uniform layer and measuring a partially sublimated surface.

A few other alternative methods have been used to obtain the heat transfer coefficient on the rib surface. Liou and Hwang [30] used holographic interferometry to measure the temperature gradient of the heat transfer medium near the surface of the rib. This method provides spatially resolved convection coefficients around the perimeter of a simple two-dimensional rib. This method results in a large uncertainty because of the inherent difficulty in measuring the change in air temperature so close to the surface. Nirmalan et al. [31] used IR imaging to measure the temperature outside the backside wall of an as-manufactured part to re-generate the channel side heat transfer coefficients. The predicted internal heat transfer coefficient distribution was applied to a finite element model to computationally determine the external surface temperature. This process is repeated until the computationally predicted external temperatures match the experimentally measured external temperatures. This method is beneficial in that it is non-destructive; however, the heat transfer coefficients on specific internal features cannot be fully resolved.

In addition to experimentally resolving the convection coefficient on the rib, many researchers have used computational fluid dynamics (CFD) to predict a convection coefficient distribution along a ribbed passage [32-35]. Various turbulence models have been used and have shown good agreement with experimental data.

NEW MEASUREMENT METHODOLOGY

Two heat transfer measurement methods will be discussed. The first method is the newly developed methodology, and the second is the validation methodology that is based on a proven test method [15-17] and discussed later.

The premise for the new method was to make use of a lumped mass approximation by ensuring Biot numbers much less than unity. Because complex geometries were an objective of the study, it was important to find a material that could be easily fabricated into complex shapes yet retain a high thermal conductivity to match the Biot requirement. Through an uncertainty analysis, it was noted that any conductive heat losses must be minimized to ensure an accurate measurement.

Typical models for studying ribbed channels are made using Stereolithography Apparatus (SLA) materials which have relatively high thermal conductivity leading to lateral losses from the rib to the endwall. To prevent these losses, a number of computational predictions led to a design that consisted of a rib resting on a foam endwall with an air gap placed directly beneath the rib as shown in Figure 1.
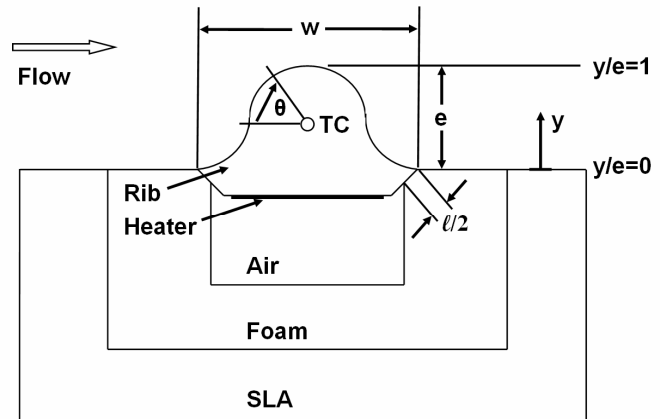

Figure 1. Schematic of new methodology.

The properties of several candidate materials for the rib and the endwall are shown in Table 1. Copper, having the highest thermal conductivity and lowest Biot numbers, is an ideal choice for the rib. Machining copper ribs with complex shapes is costly and time consuming and, as such, was not used for this methodology. Instead, ribs were cast from Indium alloys (Indalloy) that feature a high thermal conductivity and low melting temperature. The low melting temperature allows for safer and more economical castings when compared with traditional casting materials and methods, such as copper and aluminum. Using negative molds allows the manufacturing of ribs that are varied in shape, which significantly reduces the time and cost required to machine a rib in comparison with conventional machining methods.

Table 1. Material Properties for Rib and Endwall

	k [W/m·K]	T_{melt} [F]	Bi Re=1.0e4	Bi Re=1.0e5
Foam	0.037	-	3.7	15.1
SLA	0.25	-	0.5	1.9
Indalloy 1	17	281	0.006	0.02
Indalloy 2	73	290	0.001	0.006
Indalloy 3	86	313	0.001	0.005
Copper	401	1984	0.0003	0.001

3

To validate the Biot number calculations and predicted measurement error, a two-dimensional ANSYS model was used. The convection coefficient applied to the endwall was assumed to be that of a smooth channel determined using the Dittus-Boelter correlation for each Reynolds number [35]. The convection coefficient on the rib was assumed to be uniform and equal to five times the smooth channel convection coefficient for Reynolds numbers ranging from 10,000 to 100,000 [32]. An adiabatic condition, achieved experimentally by insulating the test model from ambient conditions, was applied to the non-flow side of the model. Finally, a uniform heat flux was applied to the bottom of the rib.

The temperature uniformity was checked using a non-dimensional temperature defined in equation 1,

$$\theta = \frac{T - T_\infty}{T|_{y/e=0.5} - T_\infty} \qquad (1)$$

where the computed non-dimensional temperature was plotted along the centerline of the two-dimensional rib from the endwall, $y/e = 0$, to the wetted surface, $y/e = 1$. The temperature was normalized using the temperature at the center of the rib. Figures 2a and 2b show a comparison of the temperature uniformity between various rib materials at Re = 10,000 and Re = 100,000 respectively. For the Indium alloys, the rib temperatures are nearly uniform at Re = 10,000 and show only a slight gradient at Re = 100,000. The temperature profile in the copper rib is essentially uniform for the range of Reynolds numbers due to such a high thermal conductivity. Despite the change in uniformity with Reynolds numbers, the Indium alloys perform similarly well. And, the temperature uniformity of each alloy is proportional to thermal conductivity. Indalloy #2 was chosen for further analysis based on thermal performance, melting temperature, and cost.

After selecting a rib material, the design of the endwall and air cavity was evaluated with the goal of minimizing the percent heat loss to conduction. The features of each design iteration are summarized Table 2. The first two designs employ a rib resting on an SLA endwall. Design #1 uses an SLA rib (for comparison purposes) and design #2 uses Indalloy #2. It was noted that placing the heater at the interface between the rib and the SLA led to excessive conduction losses. As such, a portion of the SLA endwall was replaced with an air gap for design #3. The contact length, ℓ/w, is defined as the contact length of rib material to the endwall divided by the width of the rib. This length was found to have a large impact on the heat lost to conduction as shown when an air gap was added to the model. To further reduce the contact length, the geometry of the rib was modified for design #4 as shown in Figure 3. In addition to reducing the contact length, design #4 makes casting the ribs easier by removing the sharp corners in design #3. For design #5, a portion of the SLA endwall adjacent to the rib was removed and replaced with foam making the entire contact length of the rib in contact with either foam or air (Figure 1).
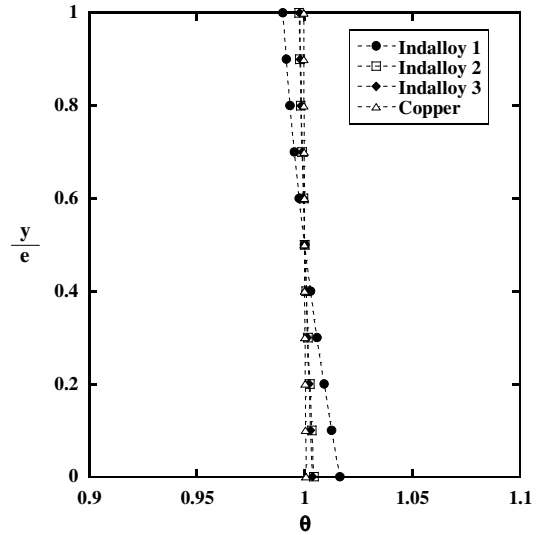

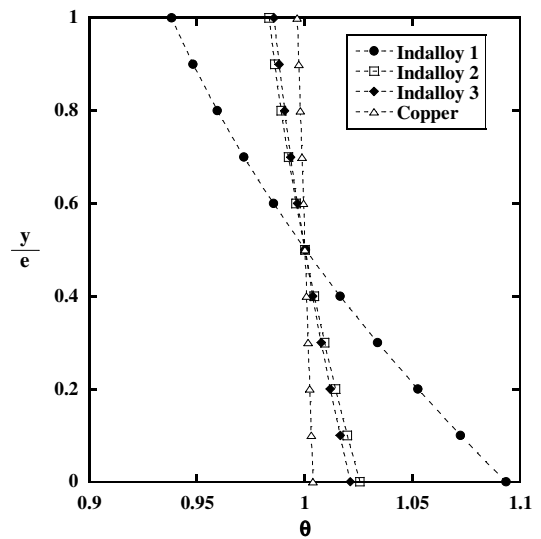**Figure 2a. Non-dimensional temperature along the rib centerline at Re = 1.0e^4.**

Figure 2b. Non-dimensional temperature along the rib centerline at Re = 1.0e^5.

Table 2. Summary of Design Iterations Tested with Two-Dimensional Model

Design	Contact Length (l/w)	Rib Material	Gap Material	Insulating Features
1	0.40	SLA	SLA	None
2	0.40	Indalloy 2	SLA	None
3	0.22	Indalloy 2	Air	None
4	0.15	Indalloy 2	Air	None
5	0.15	Indalloy 2	Air	Foam

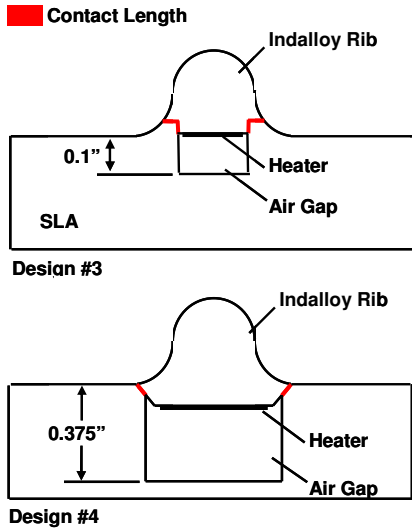4   Copyright © 2008 by ASME

Figure 3. Two successive design iterations showing a reduced contact length for the new methodology.

The percent heat loss to conduction through the endwall for the various design iterations is shown in Figure 4. By adding an air gap, reducing contact length, and replacing the SLA endwall with foam, the percentage of heat lost to conduction was reduced from approximately 50% to within 10% at all Reynolds numbers of interest.

Contour plots of the non-dimensional temperature distribution, as shown in Figure 5, show the reduction in conductive heat loss with each design change. Again, by adding an air gap, reducing contact length, and placing the rib atop a foam endwall (design #5) the lateral conduction is drastically attenuated.
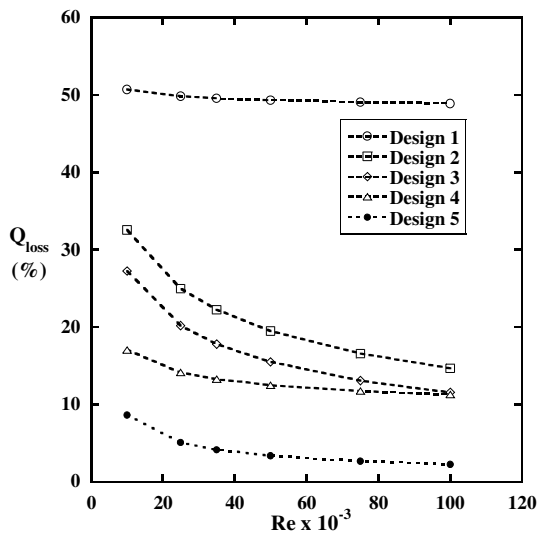
Figure 4. Percent heat loss versus Reynolds number for the two-dimensional ANSYS model.
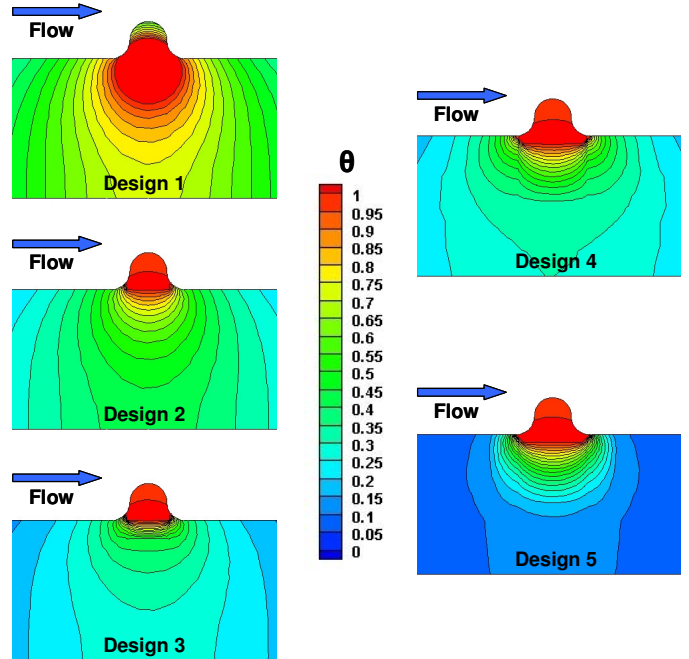
Figure 5. Non-dimensional contour plots for various design iterations at Re = 1.0e^4.

A three-dimensional model, shown in Figure 6, was created to determine the effect of a spatially varying rib convection coefficient. Also, the three-dimensional model was used to predict the conductive losses in order to correct experimental measurements (to be discussed later).
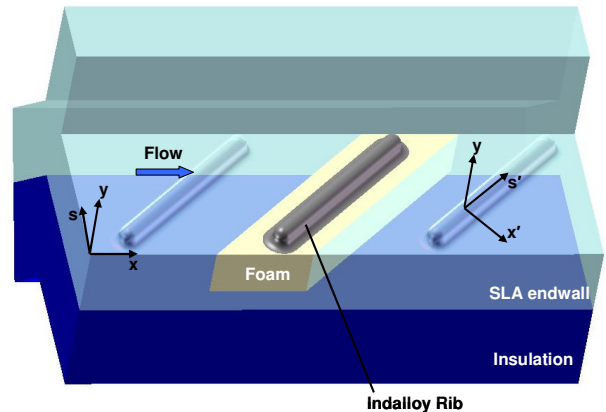

Figure 6. Three-dimensional ribbed model.

Before modeling the full three-dimensional geometry in ANSYS, it was compared with the two-dimensional model with respect to conduction losses. It should be noted that an alternate coordinate system has been defined to simplify data presentation. The spanwise variable, s, and the streamwise variable, x, have been rotated 45° clockwise about the y-axis. The new coordinate system, denoted with primes, is aligned with the rib in the s′ direction. The boundary conditions were similar to the two-dimensional model. In the three-dimensional

5   Copyright © 2008 by ASME

model, the rounded rib ends are not adiabatic, as with the assumption of a two-dimensional simulation. Adiabatic conditions are placed at the symmetry planes and on the non-flow sides of the model. Several grid refinements were analyzed to ensure a grid independent solution, and there was less than 1% change in conduction losses between the two finest grids.

Figure 7 shows a comparison of the percent heat loss between the two- and three-dimensional models. The two models follow the same trend. The three-dimensional model exhibits a slight increase in conductive losses due to the end effects mentioned previously.
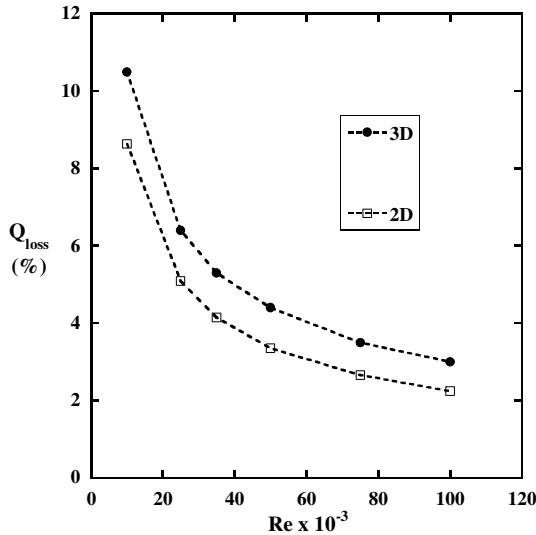
Figure 7. Comparison of percent heat loss between the two- and three- dimensional models.

All of the previous results have used a constant convection coefficient on the rib surface at an assumed augmentation factor of five. Computational predictions indicate that a non-uniform convection coefficient is present on the rib surface [32]. As such, a spatially varying convection coefficient distribution was applied to the three-dimensional model. The spatially varying convection coefficient, derived from literature, was discretized circumferentially [36] and in the spanwise direction [32]. The variation in augmentation in both the circumferential direction and spanwise direction is shown in Figure 8 for Re = 100,000. Similar distributions were used for the other Reynolds number calculations only scaled appropriately for the Reynolds number.

Both a uniform and a spatially varying convection coefficient distribution were analyzed with the three-dimensional model. Both cases have equivalent area-averaged augmentation factors ranging from 7.1 to 3.5 for Reynolds numbers of 10,000 to 100,000, respectively. The amount of heat lost to conduction for the two distributions is shown in Figure 9. The losses for each case are nearly equal, yet show a slight offset due to end effects. At the ends of the rib, the curvature creates additional surface area for convection in an area with an already enhanced augmentation. With respect to

circumferential location, the large stagnation region at the leading end of the rib is subject to a large augmentation factor. And, with respect to spanwise location, the leading end of the rib is subjected to large augmentation as a manifestation of the strong secondary flows which decay along the span of the rib toward the trailing end. Despite having equal area-averaged heat transfer augmentation, the spatially varying distribution shows less heat loss due to the effect of high augmentation at the leading end of the rib where there is more surface area for heat transfer.
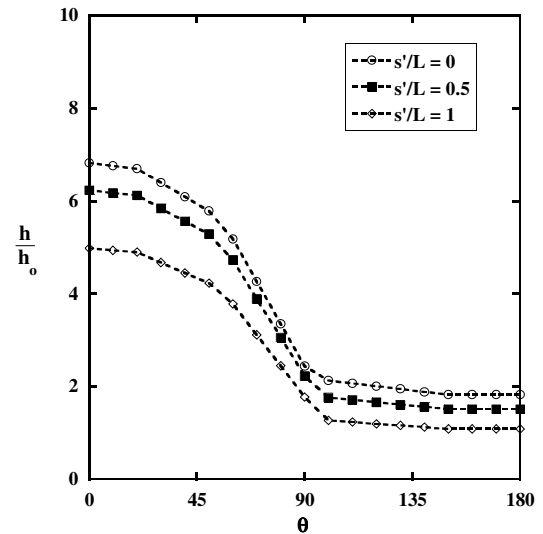

Figure 8. Variation in augmentation factor for various circumferential and spanwise locations for Re = 1.0e^5.
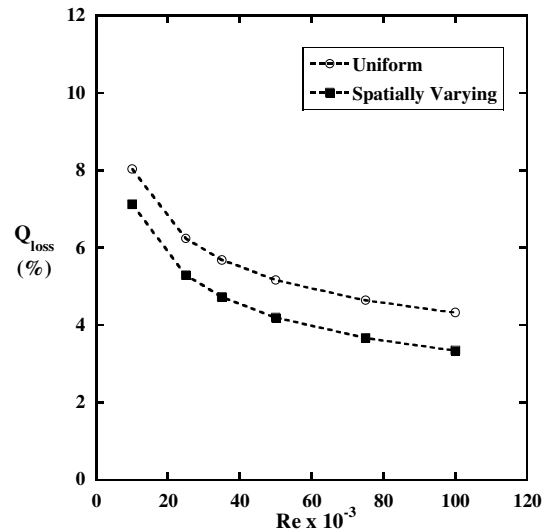

Figure 9. Percent heat loss versus Reynolds number for different convection coefficient distributions.

Figure 10 shows the non-dimensional temperature along the centerline of the rib for both boundary conditions. This plot illustrates the effect of a spanwise varying convection

6   Copyright © 2008 by ASME

coefficient. For the uniform convection coefficient, the non-dimensional temperature is symmetric about s′/L = 0.5 with lower temperatures at the rib ends due to the increased convective area. Conversely, the spatially varying convection coefficient results in a spanwise temperature gradient where the leading end of the rib is at a lower temperature than the center due to a large convective area combined with the large augmentation factors mentioned previously. The decaying strength of the secondary flow causes the spanwise temperature gradient. The temperature drop at the trailing end of the rib is caused by the increased convective area. The effects of varying convection coefficient circumferentially were observed by plotting the non-dimensional temperature across the midspan of the rib (s′/L = 0.5), shown in Figure 11. The higher convection coefficient on the leading side of the rib, where stagnation occurs, results in lower temperatures than the trailing side of the rib, where flow separation inhibits convective heat transfer.
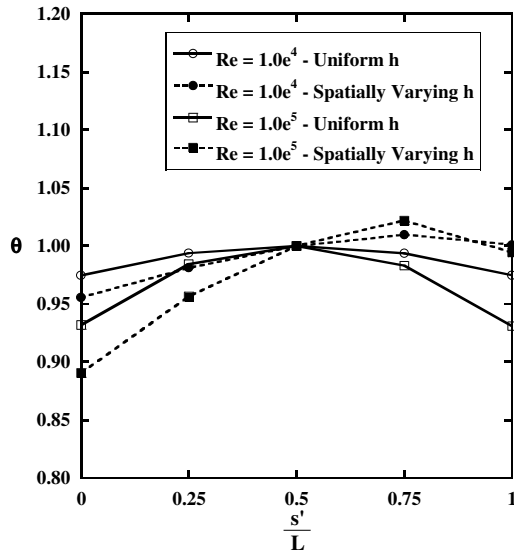
As shown with both the two- and three-dimensional ANSYS models, a rib material that satisfies the Biot number criteria can still show strong temperature variation when subject to convection coefficients typical of internal cooling applications. As such, the three-dimensional model was used to estimate the accuracy of quantifying the area-average surface temperature using internal rib temperatures. Experimentally, thermocouples embedded in the rib were used to measure the integrated convection coefficient, which is defined as the area-averaged convection coefficient on the rib surface. The error of the measured convection coefficient is defined as the percent difference between the integrated convection coefficient applied as a boundary condition in the ANSYS model and the convection coefficient measured by a point temperature in the rib. An experimental temperature measurement was approximated by taking the average temperature of a cluster of nodes. The radius of the node cluster was assumed to be the same size of the thermocouple bead.

To account for tolerances in the instrumentation process, the thermocouple was offset by 25% of the rib height in various directions from the center of the rib. The offset thermocouple locations are shown in Figure 12. It should be noted that when the experiments were conducted, five thermocouples were placed along the span of the rib, as shown in Figure 13, to obtain an average temperature.

Figure 10. Non-dimensional temperature along the span of the rib (three-dimensional model, y/e = 0.5).

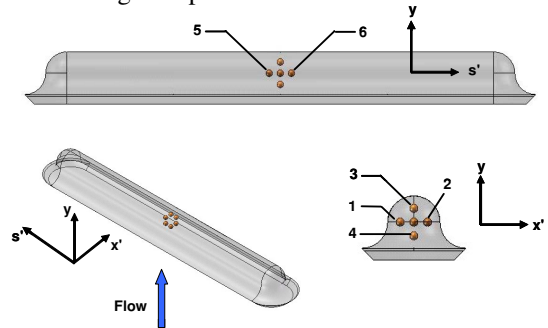**Figure 12. Thermocouple locations within 3D ANSYS model for checking location sensitivity.**

Figure 11. Non-dimensional temperature contours (three-dimensional model, s′/L = 0.5).
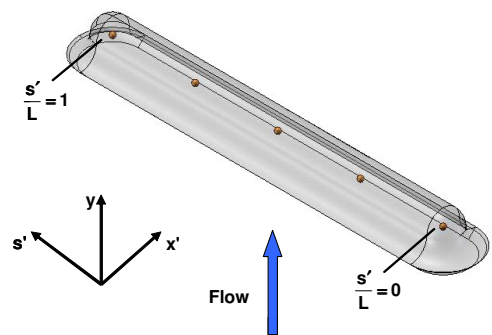
Figure 13. Thermocouple locations used experimentally to determine rib-averaged convection coefficient.

7   Copyright © 2008 by ASME

Figure 14 shows the error of the measured convection coefficient based on different thermocouple locations. It is immediately apparent that using five thermocouples quantifies the integrated convection boundary condition more accurately than using a single point measurement. By moving a single point thermocouple in various directions the error in the convection coefficient can vary between 3.0% and 4.4% at Re = 100,000. Using five span-averaged thermocouples brings the overall error to within 1%. Therefore, the use of five span-averaged thermocouples delivers an accurate integrated convection coefficient at all Reynolds numbers of interest.
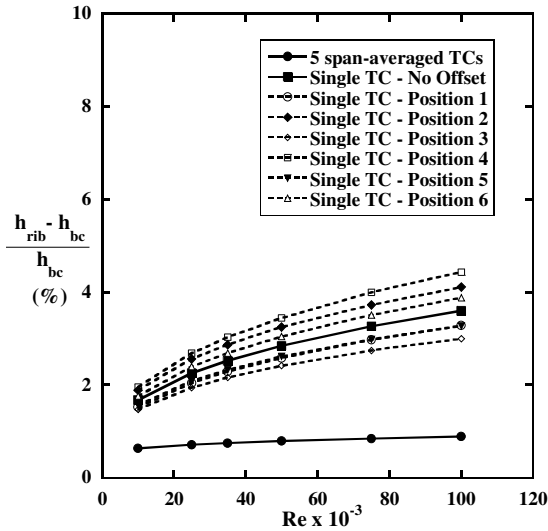

Figure 14. Measurement error for different thermocouple locations.

In summary, the design of the new methodology revolves around several key features. First, the temperature uniformity of the lumped model was verified. Second, lateral losses were minimized by insulating the rib with a foam endwall and an air gap. Finally, variations in local convection coefficients were shown to have a minimal impact on the ability to quantify the integrated surface temperature.

VALIDATION METHODOLOGY

The validation methodology was similar to those experimental setups described previously that overlay a foil heater atop an insulated surface [15-17]. The heater provided constant heat flux on the convective surface while the insulated endwall minimized conductive heat losses through the back of the heater. The area-averaged rib heat transfer coefficient was found by integrating local surface temperature measurements.

A schematic of the validation method is shown in Figure 15. As with the new method, ANSYS was used to predict the conductive heat losses. Since the path from heat generation to convection is less resistive than the new method, the percentage of heat input lost to conduction is less than 5% at all Reynolds numbers.
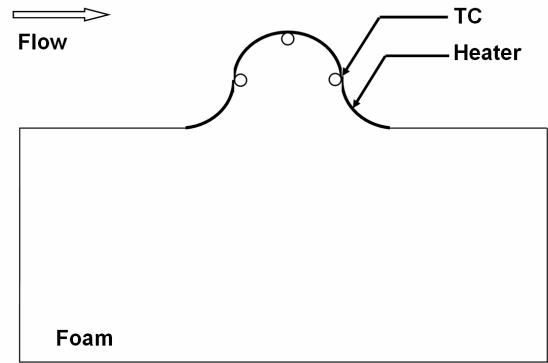

Figure 15. Schematic of validation methodology.

EXPERIMENTAL FACILITY

Experiments were conducted in a closed-loop, re-circulating channel. The experimental facility, documented by Lyall et al. [18], is shown schematically in Figure 16. Flow originates at the blower and travels along the re-circulation portion of the rig where it encounters an inlet plenum. The inlet plenum is equipped with a splash plate to prevent jet formation and a heat exchanger to maintain constant inlet temperature at nominally ambient temperatures. The flow then exits the plenum into the hydrodynamic entrance region. This entry region is over 35 hydraulic diameters which ensures a fully developed flow for all Reynolds numbers of interest. The flow then passes through the ribbed channel where heat transfer measurements were made. A calibrated orifice meter was placed downstream of the test section to measure flow rate. The flow meter was installed with ten hydraulic diameters of smooth pipe upstream and six hydraulic diameters of smooth pipe downstream to ensure an accurate measurement. After passing the flow meter, the cycle is completed and the flow returns to the blower. Steady state was achieved in two hours and was signified when all thermocouples remained constant over a fifteen minute period. Data was recorded for one minute after steady state was reached.
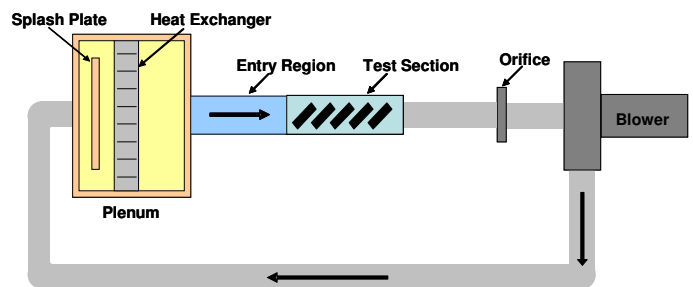

Figure 16. Schematic of experimental facility [18].

The ribbed channel test section is comprised of two opposing ribbed walls with rounded, skewed ribs oriented at 45° from the channel axis. The parameters of the test section are summarized in Table 3.

8   Copyright © 2008 by ASME

Table 3. Rib Design Used for Evaluating Testing Methods

e/D_h	0.075
P/e	8
s'/D_h	0.69
α	45°
AR	1.7:1
Rib Type	skewed, rounded, discontinuous

Four rib sections were installed beginning with the sixth rib from the entrance of the test section to ensure a hydrodynamically fully-developed flow in the ribbed channel. Four different test ribs were installed consecutively in the milled pocket. Figures 17a and 17b show the foam segments placed in the SLA endwall with four test articles installed from the new method and the validation method respectively. Four different ribs were tested for each method to give an indication of any uncertainty in the manufacturing method. The methods were both used to quantify the heat transfer of a single rib. As such, the thermal boundary condition on all other ribs and endwall surfaces were adiabatic.
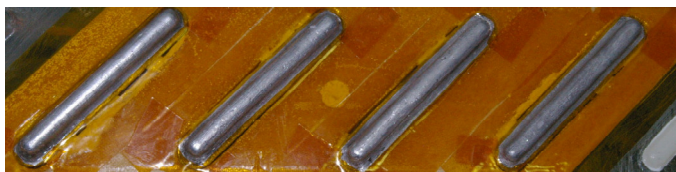

Figure 17a. Large scale ribbed model with four Indalloy ribs placed in a foam endwall.

Figure 17b. Large scale ribbed model with four foam ribs encased in Inconel foil.

The description of implementing the new method begins with the rib. First, the rib was cast by melting the Indium alloy in a conventional oven. The molten mixture was then poured into a mold of the desired rib geometry. After solidifying, the rib was removed from the mold. The rib was then polished to remove any casting imperfections and to reduce any possible radiative losses. A 3-axis mill was used to precisely drill holes and cut grooves for thermocouples and lead wires to reside in. The volume removed by the grooves is less than 2% of the uncut rib volume meaning the Biot number will not be affected. Five 36AWG Type E thermocouples with Neoflon PFA sheathing were then secured in the cavities using thermally conductive but electrically insulating cement. The wires were then laid along the grooves and all gaps were filled with thermally conductive cement to prevent air pockets in the rib. A strip of Inconel foil was used as the heating element for the new methodology. Two copper lead wires were soldered to the Inconel foil before adhering the heater to the rib with Kapton tape. Next, the foam endwalls were cast in an SLA mold. To ease the removal of the foam, the casting surface of the mold was covered with Teflon-coated tape and mold release resin prior to pouring the foam. A two-part urethane foam was then mixed and poured into the mold. After the foam expanded and hardened, the endwall was removed from the mold; and, the instrumented rib was installed on the foam. Extremely thin Kapton tape was used to hold the rib in place atop the foam endwall and to prevent any leaks around the rib. Finally, the rib/endwall unit was lowered into the SLA test model.

The validation method was manufactured in a similar way with the exception of the foam casting process. The Inconel heater was laid into the SLA mold and fitted with thermocouples and heater lead wires prior pouring the foam. 36AWG Type E thermocouples were adhered to the heater using thermally conductive cement. After pouring the foam, the endwall and heater were carefully separated from the mold as a single unit. It is important to note that the lead wires were essentially cast in the foam, and the wires exit the backside of the foam endwall. The final unit is lowered into the SLA test model as with the new method.

DATA REDUCTION

For the new methodology, a lumped model approximation was used based on the measured rib temperature taken from five thermocouples embedded along the span of the rib. The rib convection coefficients were defined in equation 2,

$$h = \frac{Q_{heater} - Q_{loss}}{A(T_{rib} - T_\infty)} \quad (2)$$

where T_{rib} is the average of five thermocouples embedded in the rib. The convective heat in equation 2 is equal to the amount of power dissipated by the heater less conductive losses. It is important to note that radiation contributions were estimated and found to be less than 1% of the total heat transfer applied; therefore, radiation was neglected. In addition, radiation was computed using ANSYS with air and with a vacuum beneath the heated rib. Results indicated negligible differences in the rib temperatures. Many experimental setups permit the use of a one-dimensional conduction model to quantify losses. Due to the significant contribution of lateral conduction, losses were accounted for using ANSYS. These loss calculations from ANSYS were made by experimentally measuring the area-averaged convection coefficient assuming no heat loss. The no-loss convection coefficient was then applied to the three-dimensional ANSYS model to obtain a heat loss estimate. The resulting conductive loss was used to correct the no-loss convection coefficient. Finally, augmentation factors were calculated based on the Dittus-Boelter correlation [37].

9 Copyright © 2008 by ASME

In order to use ANSYS to correct for conduction losses, the model was first verified using experimental data. Figure 18 shows the non-dimensional temperature, θ, along the span of the rib comparing ANSYS to the new methodology for Re = 10,000 and Re = 100,000, respectively. It should be noted that the convection coefficient applied to the rib was taken from experimental data assuming no heat loss and was applied with variations in the spanwise direction only. The non-dimensional temperature along the span of the rib matches well between the ANSYS model and the experimental data collected using the new method. The agreement between the predicted and experimental temperature profiles warrants the use of the predicted percent heat loss in the heat transfer coefficient calculations.
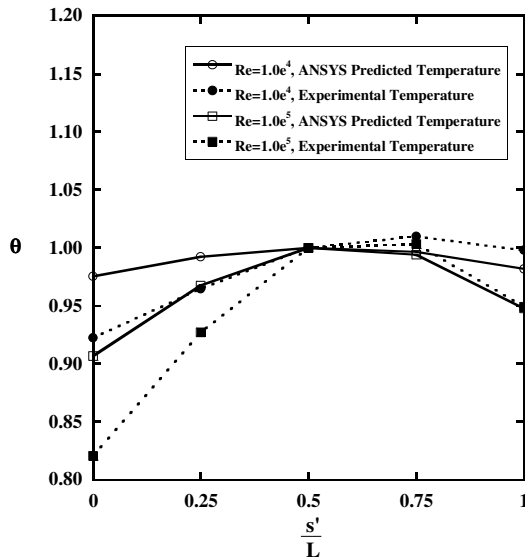

Figure 18. Non-dimensional temperature at center of rib (y/e = 0.5) captured at various spanwise locations for Re = 1.0e^4 and 1.0e^5.

For the validation methodology, convection coefficients were measured locally at different locations on the rib. Local convection coefficients were calculated using equation 2 where T_{rib} was the temperature of a single thermocouple. The rib-averaged convection coefficient was found by integrating the local convection coefficients across the rib surface. As with the new method, ANSYS was used to predict the heat losses in equation 2.

UNCERTAINTY ANALYSIS

Augmentation factor uncertainty was calculated for every Reynolds number tested using the method described by Kline and McKlintock for both measurement methods [38]. For the new method, uncertainties in augmentation factor ranged from 5.3% to 4.6% at Reynolds numbers of 25,000 and 100,000, respectively. For the validation method, uncertainties in augmentation factor ranged from 5.1% to 2.4% at Reynolds numbers of 25,000 and 100,000, respectively.

COMPARISON OF NEW AND VALIDATION METHODS

Prior to comparing all the results, a series of experiments were conducted to determine the repeatability of each method. These tests were specifically conducted to determine the sensitivity to the manufacturing methods used. Figure 19 shows the augmentation factor for both methods where the conduction losses were predicted and accounted for using ANSYS. The augmentation results agree between the four ribs and the two methods as shown by the augmentation factors falling within a mean value bounded by the respective uncertainty levels.
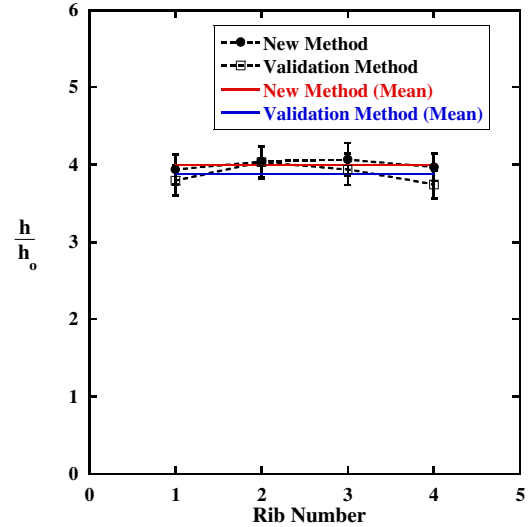

Figure 19. Augmentation factor of four ribs using the new and validation methods (Re = 2.5e^4).

The results in Figure 20 show that both the new and validation methods agree, within the experimental uncertainty, for the full range of Reynolds numbers tested. For clarity, error bars are shown on the lowest and highest Reynolds numbers. Both methods show that augmentation factor decreases with Reynolds number, which is consistent with the augmentation factors derived from literature that were applied to the ANSYS model. The nature of ribbed channel flow is such that at low Reynolds numbers, higher augmentations in friction factors and heat transfer occur. At lower Reynolds numbers, turbulators substantially alter the flow to become fully turbulent. Conversely, at higher Reynolds numbers, the flow is already fully turbulent and thereby the turbulators do not significantly enhance the convective transport.

Taslim et al. [11] experimentally determined the area-averaged rib surface convection coefficient for a 45° round-corner rib between Re=10,000 and Re=50,000. Vishwanathan et al. [32] performed a large eddy simulation for a geometry similar to the current work at Re = 25,000. Table 4 lists the geometric parameters for each study. Both the computational and experimental results agree well with the data we show in Figure 20.

Table 4. Comparison of Rib Geometries

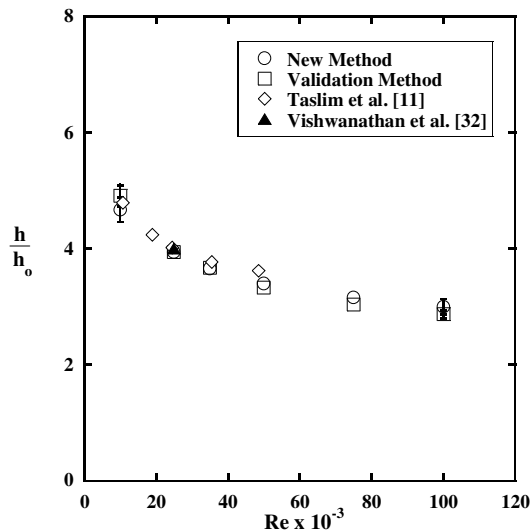|	Current Study	Taslim et al. [11]	Vishwanathan et al. [32]
Rib Profile	⌢	⊓	⌢
Continuous	No	Yes	Yes
e/D_h	0.075	0.133	0.1
P/e	8	8.5	10
α	45°	45°	45°

Figure 20. Augmentation factor for new and validation methodology.

CONCLUSIONS

As ribbed channels become increasingly complex, a new method for measuring the heat transfer coefficients for complex rib shapes is desired. Moreover, it is instructive to understand how the rib heat transfer coefficients compare with the endwall heat transfer coefficients. Many past studies have used copper ribs whereby the endwall and rib contributions to the heat transfer enhancement were lumped into an overall channel-average. Machining copper ribs to match the desired complex shape is time-consuming and difficult. The goal of the current work was to determine an alternative testing method that would provide accurate results for complex rib shapes.

A new method was developed to resolve heat transfer contributions from complex ribbed surfaces. The new method makes use of a rib material that has similar properties to copper but is more readily castable. The material that was identified, Indalloy #2, is unique in having a high thermal conductivity and a low melting temperature which makes the use of negative molds possible. These properties allowed for a lumped mass approximation which was validated computationally and experimentally.

Another critical part of the methodology was to reduce the conductive losses, ultimately reducing the experimental uncertainty. The conductive losses were minimized by insulating the heated rib with an air gap and an endwall cast from low thermal conductivity foam. These insulating features reduced the losses from approximately 50% to within 10% at all Reynolds numbers. In addition to designing for minimal heat loss, ANSYS was used to predict the amount of conductive losses by correcting the experimental convection coefficient with the predicted conduction losses. The predicted losses were obtained by applying an experimentally determined convection coefficient to the ANSYS model.

The new measurement method was validated by comparing the heat transfer results to an experimentally proven validation method. The two methods agree; and, the data presented in the current work agrees with work done by previous researchers. Moreover, the same results were measured for all of the ribs tested making the new method independent of any manufacturing imperfections. It is important to note that in the definition of the heat transfer coefficient, the bulk temperature was used as the reference temperature since only a single rib was heated.

Internal cooling is an important technology for maintaining turbine airfoil life. Turbulated channels are commonly used to increase heat transfer by generating turbulence and providing greater surface area. The new experimental method presented in this paper for determining the rib contribution to the convective heat transfer in a ribbed channel can now be used to assess whether further enhancements in heat transfer can be gained from complex rib shapes.

REFERENCES
[1] Liu, Y.H., Huh, M., Han, J.C., Chopra, S., 2007, "Heat Transfer in a Two-Pass Rectangular Channel (AR=1:4) Under High Rotation Numbers," GT2007-27067.
[2] Han, J.C., Zhang, Y.M., 1992, "High Performance Heat Transfer Ducts with Parallel Broken and V-shaped Broken Ribs," *Int. J. Heat Mass Transfer*, vol. 35, No. 2, pp. 513-523.
[3] Fu, W.L., Wright, L.M., Han, J.C., 2004, "Heat Transfer in Two-Pass Rotating Rectangular Channels (AR=1:2 and AR=1:4) with 45° Angled Rib Turbulators," GT2004-53261.
[4] Wright, L.M., Fu, W.L., Han, J.C., 2004, "Thermal Performance of Angled, V-shaped, and W-shaped Rib Turbulators in Rotating Rectangular Cooling Channels (AR=4:1)," *J. Heat Transfer*. vol. 126, pp. 604-614.
[5] Liu, Y.S., Wright, L.M., Fu, W.L., Han, J.C., 2006, "Rib Spacing Effect on Heat Transfer and Pressure Loss in a Rotating Two-Pass Rectangular Channel (AR=1:2) With 45-Degree Angled Ribs," GT2006-90368.
[6] Zhou, F., Acharya, S., 2006, "Heat Transfer at High Rotation Numbers in a Two-Pass 4:1 Aspect Ratio Rectangular Channel With 45-Degree Skewed Ribs," GT2006-90391.

11   Copyright © 2008 by ASME

[7] Metzger, D.E., Haley, S.W., 1982, "Heat Transfer Experiments and Flow Visualization for Arrays of Short Pin Fins," GT1982-138.

[8] Metzger, D.E., Fan, C.S., Haley, S.W., 1984, "Effects of Pin Shape and Array Orientation on Heat Transfer and Pressure Loss in Pin Fin Arrays," *J. of Engineering for Gas Turbines and Power*, vol. 106, pp. 252-257.

[9] Chyu, M.K., Oluyede, E.O., Moon, H.K., 2007, "Heat Transfer on Convective Surfaces with Pin-Fins Mounted in Inclined Angles," GT2007-28138.

[10] Chyu, M.K., Yen, C.H., Siw, S., 2007, "Comparison of Heat Transfer from Staggered Pin-Fin Arrays with Circular, Cubic, and Diamond Shaped Elements," GT2007-28306.

[11] Taslim, M.E., Lengkong, A., 1999, "45 deg Round-Corner Rib Heat Transfer Coefficient Measurements in a Square Channel," *J. of Turbomachinery.* vol. 121, pp. 272-279.

[12] Taslim, M.E., Lengkong, A., 1998, "45 deg Staggered Rib Heat Transfer Coefficient Measurements in a Square Channel," *J. of Turbomachinery.* vol. 120, pp. 571-580.

[13] Taslim, M.E., Wadsworth, C.M., 1997, "An Experimental Investigation of the Rib Surface-Averaged Heat Transfer Coefficient in a Rib-Roughened Square Passage," *J. of Turbomachinery.* vol. 119, pp. 381-389.

[14] Korotky, G.J., Taslim, M.E., 1998, "Rib Heat Transfer Coefficient Measurements in a Rib-Roughened Square Passage," *J. of Turbomachinery.* vol. 120, pp. 376-385.

[15] Chang, S.W., Liou, T.M., Chiou, S.F., Chang, S.F., 2007, "High Rotation Number Heat Transfer of Rotating Trapezoidal Duct with 45-deg Staggered Ribs and Bleeds from Apical Side Wall," GT2007-28174.

[16] Chang, S.W. , Liou, T.M., Yeh, W.H., Hung, J.H., 2006, "Heat Transfer in a Radially Rotating Square-Sectioned Duct with Two Opposite Walls Roughened by 45° Staggered Ribs," GT2006-90153.

[17] Ames, F.E., Dvorak, L.A., Morrow, M.J., 2007, "Turbulent Augmentation of Internal Convection over Pins in Staggered Pin Fin Arrays," GT2007-53889.

[18] Lyall, M.E., Thrift, A.A., Thole, K.A., Kholi, A., 2007, "Heat Transfer from Low Aspect Ratio Pin Fins," GT2007-27431.

[19] Ames, F.E., Nordquist, C.A., Klennert, L.A., 2007, "Endwall Heat Transfer Measurements in a Staggered Pin Fin Array With an Adiabatic Pin," GT2007-27432.

[20] Diette, C. and Arts, T., 2004, "Investigation of a High Aspect Ratio Rectangular Channel with High Blockage Ratio Round-Corner Ribs," GT2004-53163.

[21] Maurer, M., von Wolfersdorf, J., 2006, "An Experimental and Numerical Study of Heat Transfer and Pressure Loss in a Rectangular Channel with V-shaped Ribs," GT2006-90006.

[22] Maurer, M., von Wolfersdorf, J., 2007, "An Experimental and Numerical Study of Heat Transfer and Pressure Losses of V- and W-Shaped Ribs at High Reynolds Numbers," GT2007-27167.

[23] Ekkad, S.V., Han, J.C., 1997, "Detailed Heat Transfer Distributions in Two-Pass Square Channels with Rib Turbulators," *Int. J. Heat Mass Transfer.* vol. 40, No.11, pp. 2525-2537.

[24] Han, J.C., Ekkad, S.V., Huang, Y., 1996, "Measurements on Augmented Heat Transfer Surfaces Using a Transient Liquid Crystal Technique," *Process, Enhanced, and Multiphase Heat Transfer*, ed. by Festschrift, A., Bergles, A.K., (New York, New York: Begell House Inc.), pp. 339-349.

[25] Guo S.V., Jones T.V., Lock G.D., Lai C.C., Oldfield M.L.G., Rawlinson A.J., 2000, "Influence of Surface Roughness on Heat Transfer and Effectiveness for a Fully Film Cooled Nozzle Guide Vane Measured by Wide Band Liquid Crystals and Direct Heat Flux Gauges," GT2000-0204.

[26] Cho, H.H., Kim, Y.Y., Kim, K.M., Rhee, D.H., 2003, "Effects of Rib Arrangements and Rotation Speed on Heat Transfer in a Two-Duct Pass," GT2003-38609.

[27] Kim, K.M., Park, S.H., Jeon, Y.H., Lee, D.H., Cho, H.H., 2007, "Heat/Mass Transfer Characteristics in Angled Ribbed Channels with Various Bleed Ratios and Rotating Numbers," GT2007-27166.

[28] Han S., Goldstein R.J., 2005, "Influence of Blade Leading Edge Geometry on Turbine Endwall Heat(Mass) Transfer," GT2005-68590.

[29] Papa, M., Goldstein, R.J., Gori, F., 2002, "Effects of Tip Geometry and Tip Clearance on the Heat/Mass Transfer From a Large-Scale Gas Turbine Blade," GT2002-30192.

[30] Liou, T.M., Hwang, J.J., 1993, "Effect of Ridge Shapes on Turbulent Heat Transfer and Friction in a Rectangular Channel," *Int. J. Heat Mass Transfer*, vol. 36, No. 4, pp. 931-940.

[31] Nirmalan, N.V., Bunker, S.B., Hedlung, C.R., 2002, "The Measurement of Full-Surface Internal Heat Transfer Coefficients for Turbine Airfoils Using a Non-Destructive Thermal Inertia Technique," GT2002-30199.

[32] Vishwanathan, A.K., Tafti, D.K., 2005, "Large Eddy Simulation in a Duct with Rounded Skewed Ribs," GT2005-68117.

[33] Tafti, D.K., 2003, "Large Eddy Simulations of Heat Transfer in a Ribbed Channel for Internal Cooling of Turbine Blades," GT2003-38122.

[34] Guoguang, S., Teng, S., Chen, H.C., and Han, J.C., 2003, "Computation of Flow and Heat Transfer in Rotating Rectangular Channels (AR=4) with V-Shaped Ribs by a Reynolds Stress Turbulence Model," GT2003-38348.

[35] Jia, R., Sundén, B., 2003, "Prediction of Turbulent Heat Transfer and Fluid Flow in 2D Channels Roughened by Square and Deformed Ribs," GT2003-38226.

[36] Kakaç, S., Shah, R.K., Aung, W., 1987, *Handbook of Single Phase Convective Heat Transfer*, (New York, New York: Jon Wiley and Sons, Inc.)

[37] Kays, W.M., Crawford, M.E., 1980, *Convective Heat and Mass Transfer*, 2nd edition. (New York, New York: McGraw-Hill Book Company, Inc.)

[38] Kline, S.J., McKlintock, F.A., 1953, "Describing Uncertainties in Single-Sample Experiments," *Mech. Eng.* vol. 75, pp. 3-8.